Journal of Solid State Chemistry 312 (2022) 123279

Contents lists available at ScienceDirect

Journal of Solid State Chemistry

journal homepage: www.elsevier.com/locate/jssc

Optical properties of brannerite-type vanadium oxides, MV_2O_6 (M = Ca, Mg, Mn, Co, Ni, Cu, or Zn)

N. Lakshminarasimhan [a,b], Jun Li [a], Hua-Chien Hsu [a], M.A. Subramanian [a,*]

[a] Department of Chemistry, Oregon State University, Corvallis, 97331, OR, USA
[b] CSIR-Central Electrochemical Research Institute, Karaikudi, 630003, Tamil Nadu, India

ARTICLE INFO

Keywords:
Brannerites
Vanadium oxides
Solid solutions
Optical properties

ABSTRACT

The optical properties of brannerite-type oxides MV_2O_6 (M = Ca, Mg, Mn, Co, Ni, Cu, or Zn) and solid solutions synthesized by conventional high temperature solid state reaction method are compared in the present study. The structural phase transformation from pseudo-brannerite to brannerite was found at $x \geq 0.6$ in the solid solution $Ca_{1-x}Mn_xV_2O_6$ (x = 0 - 1). In the new solid solution of $Zn_{1-x}Co_xV_2O_6$ (x = 0 - 1), the phase transformation from brannerite to NiV_2O_6-type occurred at $x \geq 0.8$. A systematic decrease in the optical band gap with increasing Mn content in $Ca_{1-x}Mn_xV_2O_6$ resulted in the change in the colors of the samples. In $Zn_{1-x}Co_xV_2O_6$, the prominent d-d transitions of Co^{2+} ion in addition to the band gap narrowing altered the colors. The variation in the colors of brannerite-type oxides can be understood based on the changes in the optical band gap, ligand-to-metal (O^{2-}-V^{5+}) and/or metal-to-metal (M^{2+}-V^{5+}) charge transfer transitions, and d-d transitions.

1. Introduction

Inorganic pigments are an important component of paints. Finding environmentally benign, highly stable, and cost-effective pigments is always a challenging task. The serendipitous discovery of $Y(In,Mn)O_3$ blue pigment with a high near infrared (NIR) reflectivity has opened up Pandora's box in searching for new colors based on oxides [1]. Efforts were made in finding new shades of colors in the hexagonal perovskite $YInO_3$ using various transition metal ions at the B-site [2]. In the structure of $Y(In, Mn)O_3$, Mn^{3+} is five-coordinated by oxygens forming a trigonal bipyramid (TBP) that is responsible for the observed intense blue color of the sample. In this perspective, the Mn^{3+}-substituted oxides $ScAlMgO_4$, $ScGaMgO_4$, $ScGaZnO_4$, $LuGaMgO_4$, $LuGaZnO_4$, and $LuGaO_3(ZnO)_2$ with $YbFe_2O_4$-type crystal structure having Mn^{3+} in TBP coordination were found to be blue in color [3,4]. Similarly, $YAlO_3$ with In, Mn, Ti, and Zn substitutions at the Al site resulted in various shades ranging from violet to purple depending on the Mn content [5]. Oxides such as $La(Ga,Mn)Ge_2O_7$, $YGa_{1-x}Mn_xO_3$, transition metal substituted α-$LiZnBO_3$ and $LiMgBO_3$ exhibiting blue, purple, and beige-red colors were also reported [6–9]. Thus, the crystal field control around the chromophore through proper choice of crystal structures allows one to fine tune the colors of these transition metal containing inorganic compounds.

Among various oxides, vanadium oxides offer certain advantages like the yellow color due to O^{2-} to V^{5+} charge transfer (c.t.) transition, ease of synthesis, less expensive, and eco-friendly nature. The structural variations are possible due to the different coordination polyhedra such as $–VO_4$, $-VO_5$, $-VO_6$, and $–V_2O_7$ that can be adopted by V^{5+} ion. Within this context, the present work focuses on understanding the optical properties of vanadium oxides with the general formula $M^{II}V_2O_6$ [M = Ca, Mg, Mn, Co, Ni, Cu, and Zn] and their solid solutions are attempted in the present work. These oxides crystallize in four different structures, namely, columbite, brannerite, pseudo-brannerite, and NiV_2O_6-type structures [10]. They exhibit temperature- and pressure-dependent polymorphism with phase transition among these structures. For example, the columbite structure is known only under high pressures. In an ideal brannerite structure, the divalent M ion is six-coordinated and the pentavalent V ion is also six (5 + 1) coordinated by oxygens where one of the V–O bonds is longer. However, in CaV_2O_6, the V^{5+} ion is five-coordinated with distorted trigonal bipyramidal geometry and this structure is known as pseudo-Brannerite type [10]. The unit cell structures of CaV_2O_6 and MnV_2O_6 are shown in Fig. 1 [11,12]. Both the MO_6 and VO_5/VO_6 form chains along the b-axis by edge-sharing of their respective polyhedra and these chains are interconnected by corner-sharing of the polyhedra. These structural features resulted in realizing interesting properties from these vanadium oxides. Recently, CaV_2O_6 has been studied as a

* Corresponding author.
E-mail address: mas.subramanian@oregonstate.edu (M.A. Subramanian).

https://doi.org/10.1016/j.jssc.2022.123279
Received 13 May 2022; Received in revised form 20 May 2022; Accepted 23 May 2022
Available online 25 May 2022

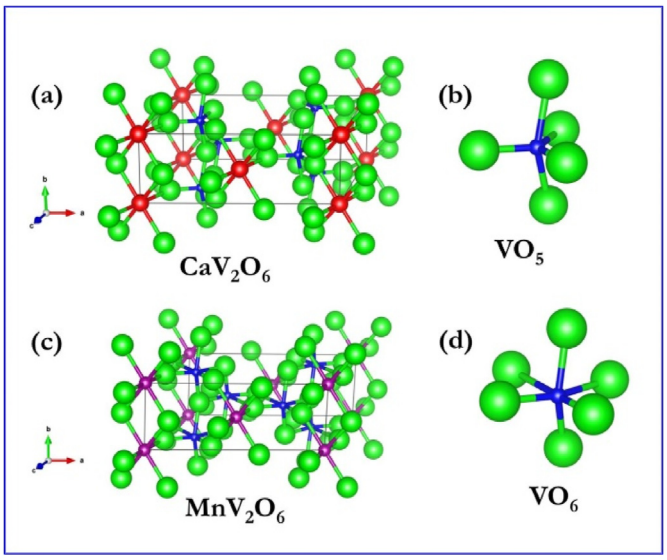

Fig. 1. The unit cell structures of (a) CaV_2O_6 and (c) MnV_2O_6 and the coordination polyhedra of V are also shown. The Ca, V, Mn and O are shown as red, blue, pink, and green spheres, respectively. The structure was drawn using VESTA software [20] based on the atomic coordinates available with Refs. 11 and 12.

spectral-converter phosphor with red emission at 630 nm [13]. Such a long wavelength emission is a unique feature ascribed to the VO_5 trigonal bipyramid with longer V–O bonds and this distinguishes CaV_2O_6 from other vanadate phosphors containing tetrahedral -VO_4 groups [13]. The compounds MnV_2O_6, NiV_2O_6, and CuV_2O_6 have been studied for their photocatalytic, photoelectrochemical, and magnetic properties [14–18]. CoV_2O_6 single crystal exhibited an unusual 1/3 magnetic plateau due to competition between interchain antiferromagnetic and ferromagnetic interactions [19]. However, the optical properties have not been studied in detail for these oxides. Thus, it is of interest to explore the optical properties of brannerite-type vanadium oxides with different transition metal ions and their solid solutions to understand the roles of band gap, charge transfer, and d-d transitions as well as the structure-optical property relationships. With this objective, here we compared the optical properties of brannerite-type MV_2O_6 (M = Ca, Mg, Mn, Co, Ni, Cu, or Zn) oxides, solid solution $Ca_{1-x}Mn_xV_2O_6$, and a new solid solution series $Zn_{1-x}Co_xV_2O_6$.

2. Experimental

2.1. Synthesis

The samples were synthesized by conventional high temperature solid state reaction method. The starting materials used were $CaCO_3$ (Alfa Aesar, 99.99%), MgO (Baker, 97%), V_2O_5 (Johnson Matthey, 99.9%), $MnCO_3$ (Alfa Aesar, 99.9%), $Co(OH)_2$ (Alfa Aesar, 99.9%), NiO (Alfa Aesar, 99.998%), CuO (Aldrich, 99.99%), and ZnO (Aldrich, 99.99%). Stoichiometric amounts of the starting materials were thoroughly ground, pelletized, and heated in air. The samples CaV_2O_6, MgV_2O_6, MnV_2O_6, NiV_2O_6, and the solid solutions $Ca_{1-x}Mn_xV_2O_6$ (x = 0 - 1) were synthesized by heating twice at 700 °C for 12 h with an intermittent grinding. In the case of CoV_2O_6, CuV_2O_6, ZnV_2O_6, and the solid solutions $Zn_{1-x}Co_xV_2O_6$ (x = 0 - 1), the synthesis temperature was 600 °C to avoid their melting [10].

2.2. Characterization

The phase formation was confirmed using powder X-ray diffraction. XRD patterns were obtained with a Rigaku MiniFlex II diffractometer using Cu Kα radiation and a graphite monochromator on the diffracted beam. Silicon powder was used as an internal standard to ensure accurate determination of unit cell dimensions. Lattice parameter refinements were carried out by Le Bail fitting using GSAS software [21,22]. The diffuse reflectance UV–Vis (DRUV-Vis) spectra of the powder samples were recorded using a spectrometer (V-600, Jasco). The L*a*b color parameters were obtained from the reflectance spectra using the spectra analysis software available with Jasco spectrometer.

3. Results and discussion

3.1. Phase formation

The phase formation of MV_2O_6 (M = Ca, Mg, Mn, Co, Ni, Cu, or Zn) samples was confirmed by powder XRD. The reflections in the XRD patterns were indexed based on the standard patterns available in the ICSD database (Fig. 2). From the difference in the XRD patterns, it is understood that CaV_2O_6 belongs to pseudo-brannerite structure and the samples MgV_2O_6, MnV_2O_6, and ZnV_2O_6 crystallize in the ideal brannerite structure [10]. CoV_2O_6 and NiV_2O_6 have NiV_2O_6-type structures whereas CuV_2O_6 exhibits the brannerite structure with a slight triclinic distortion [10,23]. Further, attempts were made to synthesize the solid solution series $Ca_{1-x}Mg_xV_2O_6$ (x = 0 - 1) and their powder XRD patterns are shown in Fig. 3. The samples exhibit CaV_2O_6 structure up to x = 0.5 and MnV_2O_6 phase in the composition region x = 0.7–1.0. The sample with x = 0.6 consists of both CaV_2O_6 (major) and MnV_2O_6 (minor) phases. Solid solutions among ideal brannerite and pseudo-brannerite structures MgV_2O_6–CaV_2O_6, ZnV_2O_6–CaV_2O_6, and CaV_2O_6–MnV_2O_6 were reported [24,25]. The lattice parameter refinement results of the CaV_2O_6 and MnV_2O_6, revealed larger lattice parameters and cell volume (Table 1) for the former compound due to the larger ionic radius of Ca^{2+} (1.0 Å) when compared to that of Mn^{2+} (0.83 Å) [26]. Compared to the MnV_2O_6 structure, one of the V–O bonds in CaV_2O_6 becomes extremely elongated owing to the larger unit cell dimensions, resulting in the bond breaking and the 5-fold coordination around V^{5+} with a distorted trigonal bipyramidal geometry as shown in Fig. 1. On the other hand, distorted VO_6 octahedral units are present in MnV_2O_6. The variations in the lattice parameters in the solid solution $Ca_{1-x}Mn_xV_2O_6$ are shown in Fig. 4. As x increases, cell edge a contracts the most upon Mn substitution, while cell

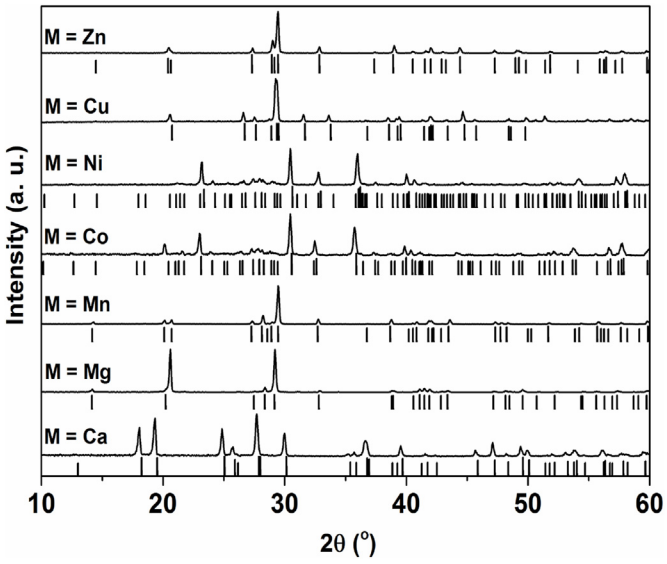

Fig. 2. Powder XRD patterns of MV_2O_6 (M = Ca, Mg, Mn, Co, Ni, Cu, or Zn) phases. The vertical lines below each pattern correspond to the standard patterns of CaV_2O_6 (01-073-0186), MgV_2O_6 (00-034-0013), MnV_2O_6 (01-072-1837), CoV_2O_6 (00-051-0130), NiV_2O_6 (01-076-2592), CuV_2O_6 (00-045-1054), and ZnV_2O_6 (01-074-1262).

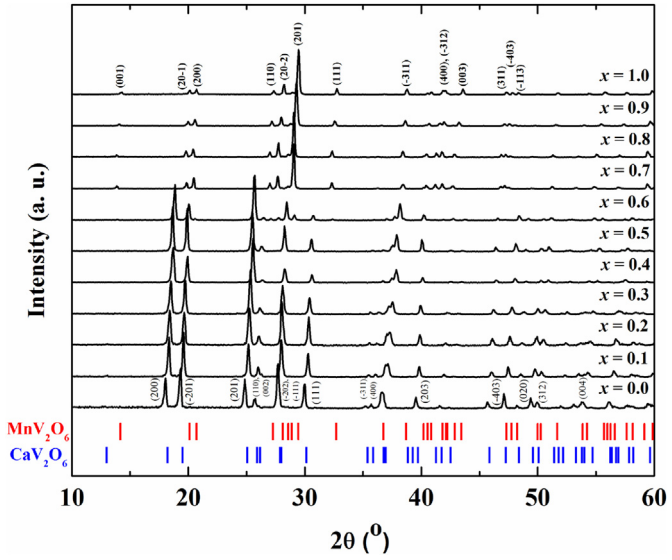

Fig. 3. Powder XRD patterns of solid solutions $Ca_{1-x}Mn_xV_2O_6$ and the standard patterns of MnV_2O_6 (01-072-1837) and CaV_2O_6 (01–073-0186) are also shown.

Table 1
Lattice parameters of select compositions in the solid solution $Ca_{1-x}Mn_xV_2O_6$.

x	*a* (Å)	*b* (Å)	*c* (Å)	*β* (°)	Space Group
0	10.049	3.671	7.033	104.85	C2/m
0.2	9.947	3.652	7.010	104.90	C2/m
0.5	9.806	3.624	6.970	104.73	C2/m
0.6	9.759	3.619	6.948	104.71	C2/m
0.7	9.334	3.553	6.851	112.56	C2/m
0.8	9.328	3.545	6.816	112.60	C2/m
1.0	9.301	3.532	6.752	112.58	C2/m

edge *c* decreases more than cell edge *b*. This lattice contraction is presumably leading to the formation of an additional V–O bond and the alteration of V coordination from VO_5 to VO_6 as approaching the Mn-rich end of the solid solution. An abrupt change in the lattice parameters can be found in the solid solution while moving from x = 0.6 to x = 0.7. It is known that CaV_2O_6 and MnV_2O_6 belong to different segments of morphotropic series and the solid solution $Ca_{1-x}Mn_xV_2O_6$ exists for x = 0 - 0.63 [25]. Thus, our results are in good agreement with the earlier report [25].

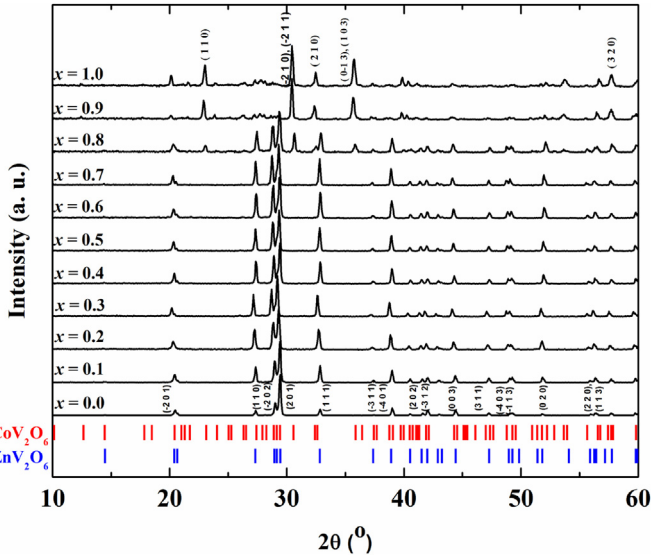

Fig. 5. Powder XRD patterns of solid solutions $Zn_{1-x}Co_xV_2O_6$ and the standard patterns of CoV_2O_6 (00-051-0130) and ZnV_2O_6 (01-074-1262) are also shown.

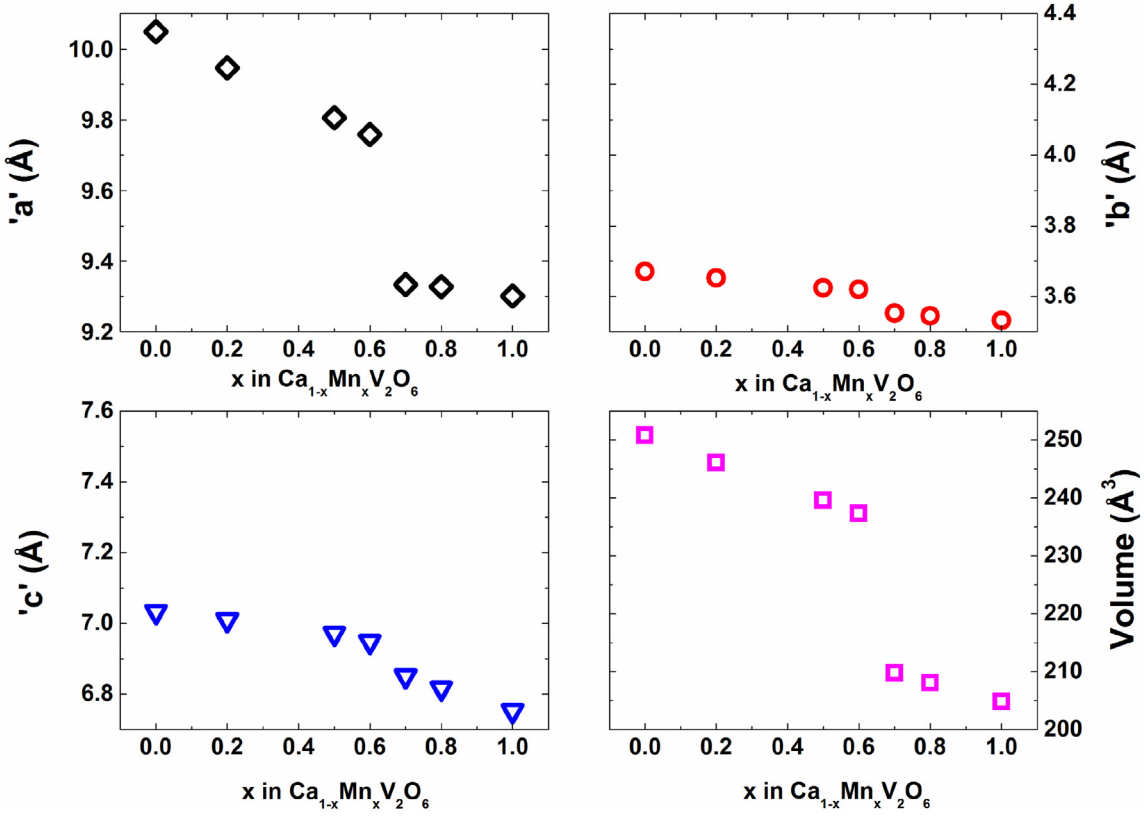

Fig. 4. Variations in the lattice parameters and unit cell volume with x in $Ca_{1-x}Mn_xV_2O_6$ solid solution.

Table 2
Lattice parameters of select compositions in the solid solution $Zn_{1-x}Co_xV_2O_6$.

x	*a* (Å)	*b* (Å)	*c* (Å)	*α* (°)	*β* (°)	*γ* (°)	Space Group
0	9.245	3.528	6.573	90.00	111.38	90.00	C2/m (monoclinic)
0.2	9.249	3.526	6.583	90.00	111.46	90.00	C2/m
0.5	9.243	3.520	6.591	90.00	111.53	90.00	C2/m
0.7	9.247	3.519	6.601	90.00	111.58	90.00	C2/m
0.9	7.169	8.896	4.811	90.14	93.52	102.17	P-1 (triclinic)
1.0	7.168	8.892	4.807	90.11	93.73	102.09	P-1

Similarly, a new solid solution series $Zn_{1-x}Co_xV_2O_6$ was also synthesized and their powder XRD patterns are shown in Fig. 5. ZnV_2O_6 belongs to a monoclinic system (space group C2/m) while CoV_2O_6 has a triclinic (space group P-1) structure [27,28]. From the XRD patterns, it is clear that the phase transformation from brannerite to NiV_2O_6-type structure occurs when $x \geq 0.8$. In the composition range x = 0.1 to 0.7, the monoclinic structure of ZnV_2O_6 is maintained and the triclinic structure of CoV_2O_6 was found for x = 0.9 while the composition x = 0.8 has a mixed phase. The variations in the lattice parameters in the $Zn_{1-x}Co_xV_2O_6$ series follow different trend in the two regions x = 0 - 0.7 and x = 0.9 and 1.0 (Table 2 and Fig. 6). For solid solution of x = 0 - 0.7, cell edge c increases with x, cell edge b decreases with x (less change than c), while cell edge a varies the least with slightly scattered data points. Based on the ionic radii of Zn^{2+} (0.74 Å) and Co^{2+} [0.65 Å (LS) and 0.735 (HS)], the lattice variation along c axis is somewhat unexpected. It is likely that Co^{2+} is more ionic than Zn^{2+} and the cation-cation repulsion induced by Co substitution would be minimized upon lattice expansion. The cell evolution in the Co-rich end (x = 0.9 and 1.0) of the solid solution is consistent with the prediction of Shannon's radii [26].

3.2. Optical properties

The MV_2O_6 (M = Ca, Mg, Mn, Co, Ni, Cu, or Zn) samples exhibited different colors as shown in Fig. 7. CaV_2O_6 is yellowish-green while ZnV_2O_6 is yellow and MgV_2O_6 is orange-yellow. The samples MnV_2O_6 and CoV_2O_6 are dark in color. The diffuse reflectance UV–Vis (DRUV-Vis) spectra of all these samples were recorded and the results are shown in Fig. 7a along with the spectrum of V_2O_5. In general, the colors can originate from d-d transitions, c. t. [ligand to metal c. t. (LMCT) or metal to ligand c. t (MLCT) and interband electron transfer], or intervalence c. t. (IVCT) [29]. For example, the red color of the Wolfram salt is due to the IVCT between Pt^{II} and Pt^{IV} [30]. In brannerite-type vanadium oxides, CaV_2O_6, MgV_2O_6, and ZnV_2O_6 both the band gap and O^{2-}-V^{5+} LMCT are responsible for their green, orange-yellow, and yellow color, respectively. With brannerite vanadium oxides based on transition metal ions like Mn^{2+}, Co^{2+}, Ni^{2+}, and Cu^{2+} with partially filled 3d orbitals, the d-d transitions are also expected to influence the colors. The absorption edge observed at 520 nm in the spectrum of CaV_2O_6 can be attributed to the c. t. band of -VO_5 and the absorption onset lies in the visible region revealing a narrow band gap. In the case of MgV_2O_6 and ZnV_2O_6, the absorption edge is red shifted when compared to that of CaV_2O_6. The absorption onset of MnV_2O_6 is further red shifted towards a higher wavelength revealing a decrease in the band gap. The largest red shift in the absorption edge accompanied by intense absorption in the near infra-red (NIR) region can be seen in the spectrum of CoV_2O_6. Except for

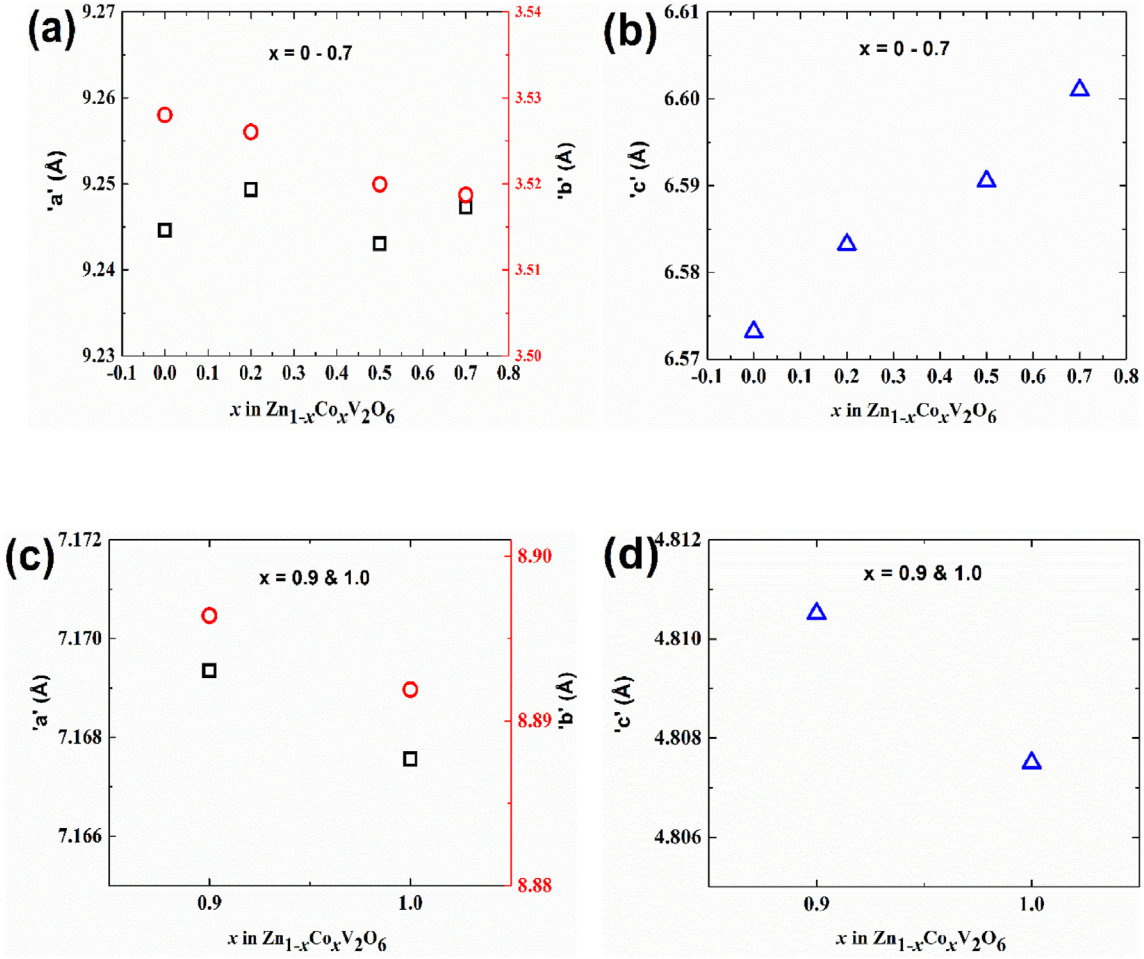

Fig. 6. Variations in the lattice parameters with x in $Zn_{1-x}Co_xV_2O_6$ solid solution for x = 0 - 0.7 (a & b) and x = 0.9 & 1.0 (c & d).

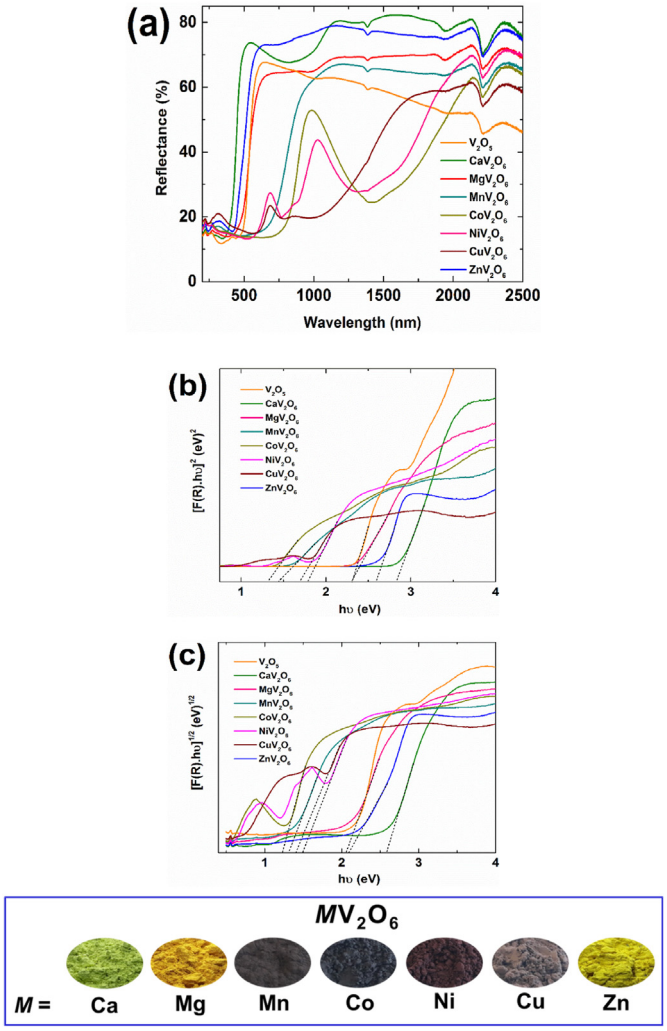

Fig. 7. (a) DRUV-Vis reflectance spectra and Tauc plots for estimation of the (b) direct and (c) indirect band gaps of V_2O_5 and MV_2O_6 (M = Ca, Mg, Mn, Co, Ni, Cu, or Zn). The photographs of the powder samples exhibiting different colors are also shown.

Table 3
The obtained optical band gap values of MV_2O_6 compounds and V_2O_5.

Compound	Band gap (eV)	
	Direct	Indirect
V_2O_5	2.30	2.06
CaV_2O_6	2.83	2.58
MgV_2O_6	2.30	2.06
MnV_2O_6	1.44	1.31
CoV_2O_6	1.31	1.23
NiV_2O_6	1.78	1.49
CuV_2O_6	1.69	1.40
ZnV_2O_6	2.60	2.09

CaV_2O_6, all the other compounds consist of six-fold coordinated V^{5+} ion while it is the distorted TBP in the former compound. CaV_2O_6 and ZnV_2O_6 have a reflectance of 75–80% in the NIR region. MgV_2O_6 and MnV_2O_6 exhibit about 65% NIR reflectance while CoV_2O_6, NiV_2O_6, and CuV_2O_6 exhibit a strong absorption in the NIR region. To understand the changes in the electronic structures with the nature of the divalent metal ions, the direct and indirect band gaps were estimated using the Tauc plots as shown in Fig. 7b. The obtained band gap values are listed in Table 3. The direct band gap of V_2O_5 is 2.30 eV and this is in agreement with the earlier reports [31,32]. It can be seen that the indirect band gap

Table 4
Color L*a*b parameters of MV_2O_6.

Compound	L	a	b
CaV_2O_6	85.069	-9.258	16.917
MgV_2O_6	67.147	8.567	27.891
MnV_2O_6	38.344	1.350	0.741
CoV_2O_6	37.058	0.073	-0.733
NiV_2O_6	38.019	6.082	1.103
CuV_2O_6	39.203	2.650	-1.619
ZnV_2O_6	78.514	-1.907	31.59

values of V_2O_5 and MV_2O_6 (M = Ca, Mg, Mn, Co, Ni, Cu, or Zn) compounds are smaller than those of the direct gap. Such an observation is similar to the earlier reported values from both the experimental and theoretical electronic structure calculations as in the case of MnV_2O_6 [14]. The band gap decreases in the order $CaV_2O_6 > ZnV_2O_6 > MgV_2O_6 > NiV_2O_6 > CuV_2O_6 > MnV_2O_6 > CoV_2O_6$. The obtained color L*a*b parameters are listed in Table 4.

A comparison of colors of complex nickel oxides including NiV_2O_6 suggested that the color and absorption in the visible region is due to the extension of charge transfer from Ni^{2+} to easily reducible V^{5+} ion into the visible region [33]. Similarly, the difference in the optical properties of NiV_2O_6, $Ni_2V_2O_7$, and $Ni_3V_2O_8$ was attributed to the different nature of vanadium polyhedra in these compounds [34]. The vanadium polyhedra (VO_5) form a chain along the b-axis by edge-sharing in NiV_2O_6 while isolated $-VO_4$ tetrahedra and $-V_2O_7$ polyhedra are present in $Ni_3V_2O_8$ and $Ni_2V_2O_7$, respectively. The different chains formed by edge sharing NiO_6 octahedra and VO_5 polyhedra along the same direction results in the d-band formation in NiV_2O_6 [34]. Hence, the electronic structures will be different among these nickel vanadates. According to ligand field theory, Ni^{2+} in an octahedral environment gives rise to three main absorptions at 1400, 800, and 400 nm due to optical transitions from ground state $^3A_{2g}$ to $^3T_{2g}$, $^3T_{1g}$(F), and $^3T_{1g}$(G), respectively [33]. The absorptions observed in the present study with NiV_2O_6 are in good agreement with this. The electronic structure calculations of CaV_2O_6 and MnV_2O_6 show that the conduction band is made up of V 3d orbitals [14,35]. In the case of MnV_2O_6, it has been found that the optical transitions are from half-filled Mn 3d orbitals and O 2p orbitals to empty V 3d orbitals [14]. Similarly, metal-to-metal charge transfer (MMCT) transitions are responsible for the observed different colors in wolframite AWO_4 (A = Mg, Mn, Co, Ni, Cu, or Zn) compounds [36]. The color of these compounds depends on the nature of the transition metal ions and their partially occupied 3d orbitals (Mn, Co, Ni, or Cu) act as the highest occupied molecular orbital (HOMO) instead of O 2p orbitals. Similarly, in the case of CoV_2O_6, NiV_2O_6, and CuV_2O_6 we can attribute the charge transfer from filled 3d orbitals of transition metal ions ($Co^{2+}/Ni^{2+}/Cu^{2+}$) and O 2p orbitals to the empty V 3d orbitals responsible for the observed colors. On the other hand, the colors of samples containing metal ions with d^0 or d^{10} electronic configurations such as CaV_2O_6, MgV_2O_6, and ZnV_2O_6 can be due to band gap and charge transfer within the VO_6 (or VO_5) groups.

To observe the influence of d-d transitions and c. t. transitions on the colors of CaV_2O_6 and ZnV_2O_6, transition metal ions with 3d electrons were substituted in $Ca_{0.99}M_{0.01}V_2O_6$ and $Zn_{0.99}M_{0.01}V_2O_6$ (M = Mn, Co, Ni, or Cu). The changes in the optical properties of the samples are shown in Fig. 8a and b. In the case of $Ca_{0.99}M_{0.01}V_2O_6$, only Mn^{2+} showed a drastic change in color while Co^{2+}, Ni^{2+}, and Cu^{2+} showed pale yellow colors. This can be understood from the optical reflectance spectra in which the $Ca_{0.99}Mn_{0.01}V_2O_6$ showed a distinct shift in the absorption onset when compared to other samples. On the other hand, in $Zn_{0.99}M_{0.01}V_2O_6$, a clear change in the colors with the introduction of different M^{2+} ions was observed and this is due to the shifts in the absorption edge to a different extent. Again, the shift is the largest for Mn^{2+} containing sample. The color change can be understood based on the introduction of d-d transitions of the substituted transition metal ions. Among these different transition metal ions, Mn^{2+} was chosen to further

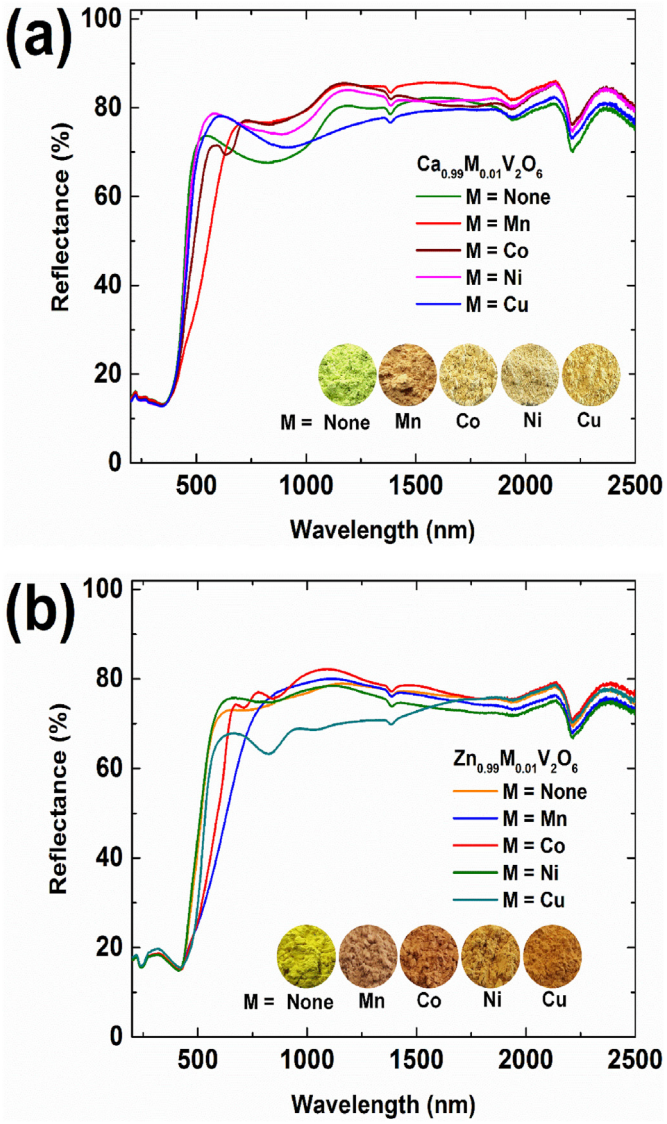

Fig. 8. DRUV-Vis spectra of (a) $Ca_{0.99}M_{0.01}V_2O_6$ and (b) $Zn_{0.99}M_{0.01}V_2O_6$ (M = Mn, Co, Ni, or Cu). The variations in the colors of the samples with different metal ions are seen from the photographs shown inside.

study the variation in the color by making the solid solution series $Ca_{1-x}Mn_xV_2O_6$. Similarly, Co^{2+} was chosen for the solid solution series $Zn_{1-x}Co_xV_2O_6$ (x = 0–1.0) as it induced a better red shade.

In the solid solution series $Ca_{1-x}Mn_xV_2O_6$, the samples exhibited a color change from yellowish-green (x = 0) to orange-red to dark brown with increasing Mn content. To understand this change in the optical properties, the DRUV-Vis reflectance spectra of the samples were recorded and the results are shown in Fig. 9a. Changes in the intensity of the c. t. absorption band of the VO_5 group in CaV_2O_6 in the region 500–1050 nm were observed with increasing Mn content and this band was almost absent in MnV_2O_6. A systematic red shift in the absorption edge with increasing Mn content is visible in Fig. 9a. This change is rationalized based on the difference in the band gaps of CaV_2O_6 (E_g = 2.83 eV) and MnV_2O_6 (E_g = 1.44 eV). The variation in the direct band gap is also shown in Fig. 9b for select compositions. The photographs of the samples show the variation in the color (Fig. 9). These variations can be due to the change in the coordination around V^{5+} from TBP to the octahedron resulting from the structural transformation from pseudo-brannerite to brannerite with higher Mn content (*see* XRD results, Fig. 3). Also, the inclusion of MMCT from half-filled Mn 3d orbitals to empty V 3d orbitals in addition to O 2p - V 3d c. t. alters the electronic structure as well as the

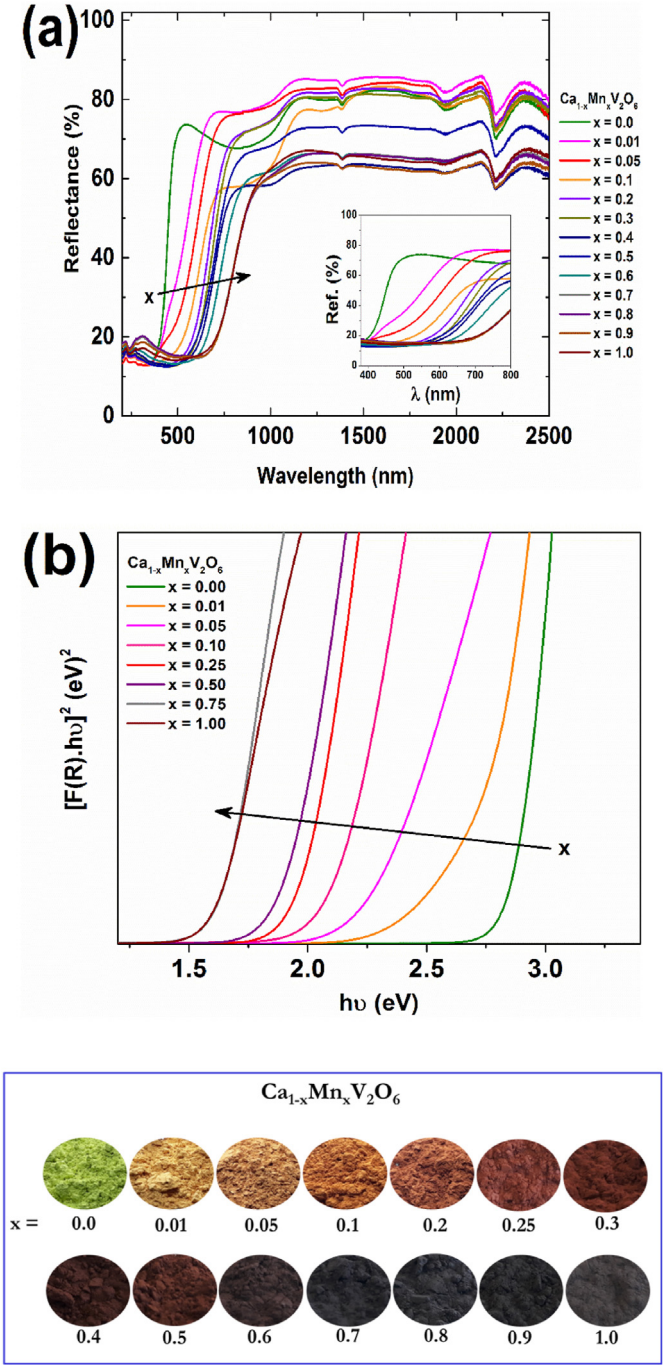

Fig. 9. (a) DRUV-Vis reflectance spectra and (b) Tauc plots showing the shift in the direct band gap of $Ca_{1-x}Mn_xV_2O_6$ samples. The photographs of the samples are also shown.

colors of the samples [14]. Thus, the variation in the colors of the samples in the solid solution is due to the band gap reduction, structural changes (VO_5/VO_6 groups), and changes in the nature of c. t. transitions. The obtained color L*a*b parameters of the compositions in the series $Ca_{1-x}Mn_xV_2O_6$ are listed in Table 5.

The DRUV-Vis reflectance and absorption spectra of $Zn_{1-x}Co_xV_2O_6$ (x = 0–1.0) are shown in Fig. 10a and b. The samples $Zn_{1-x}Co_xV_2O_6$ (x = 0.01–0.8) exhibited optical absorption bands in the regions 660–760 nm and 770–1050 nm with absorption maxima at 710 and 860 nm, respectively. These transitions can be attributed to Co^{2+} in octahedral coordination [37]. The absorption intensity systematically increased with increasing Co^{2+} content. When Co^{2+} occupies tetrahedral and/or

Table 5
Color L*a*b parameters of $Ca_{1-x}Mn_xV_2O_6$.

x	L	a	b
0.0	85.069	-9.258	16.917
0.01	71.248	8.295	22.099
0.05	60.388	12.277	17.672
0.1	50.163	12.956	13.485
0.2	43.187	11.279	8.627
0.3	40.106	9.038	5.944
0.4	39.028	6.031	4.071
0.5	40.478	7.576	6.292
0.6	37.63	3.347	1.437
0.7	38.385	0.565	-0.986
0.8	38.977	0.359	-1.014
0.9	38.623	0.461	-0.462
1.0	38.344	1.350	0.741

Table 6
Color L*a*b parameters of $Zn_{1-x}Co_xV_2O_6$.

x	L	a	b
0.0	78.514	-1.907	31.590
0.01	63.925	12.125	22.661
0.05	49.956	15.951	13.048
0.1	45.239	14.847	9.039
0.2	42.172	12.953	6.268
0.3	41.573	10.922	4.728
0.4	40.364	10.638	4.298
0.5	39.972	9.721	3.314
0.6	40.028	8.981	2.746
0.7	39.260	9.032	2.910
0.8	37.410	4.233	1.400
0.9	38.028	0.258	-0.604
1.0	37.058	0.073	-0.733

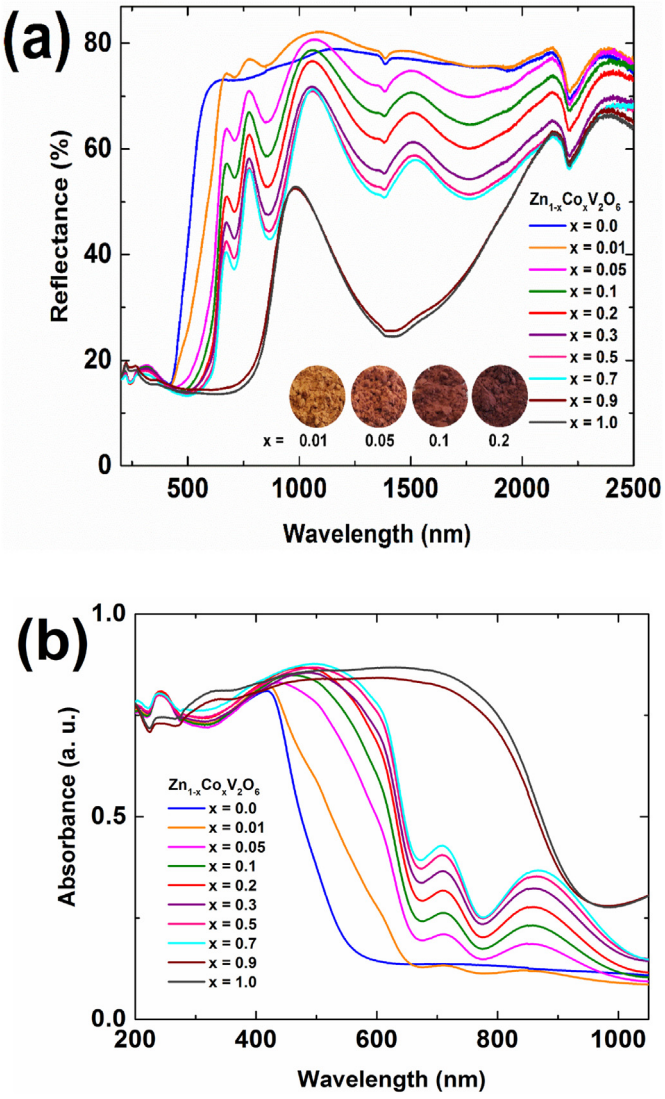

Fig. 10. (a) DRUV-Vis reflectance and (b) corresponding absorbance spectra of solid solution series $Zn_{1-x}Co_xV_2O_6$ showing the absorptions of Co^{2+} in the region between 600 and 1050 nm. The photographs in (a) reveal the change in the colors of select compositions.

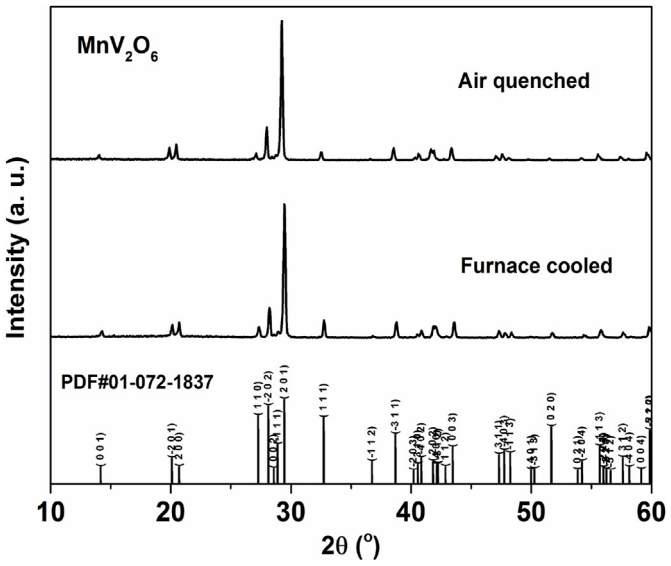

Fig. 11. A comparison of powder XRD patterns of MnV_2O_6 samples obtained by furnace cooling and air quenching. The standard pattern (01-072-1837) is also shown as a reference.

trigonal bipyramidal coordination, the optical absorption occurs between 500 and 675 nm giving rise to intense blue color as observed in hibonite, $CaAl_{12-2x}Co_xTi_xO_{19}$ [38]. Thus, the presence of Co^{2+} in octahedral coordination in the brannerite-type oxide is confirmed from the absence of any blue color in $Zn_{1-x}Co_xV_2O_6$. Further, the spectra of $Zn_{0.1}Co_{0.9}V_2O_6$ and CoV_2O_6 are different from other samples and the optical absorption onset is at 950 nm and there are no specific absorption bands of Co^{2+} as observed in the spectra of other compositions. This difference is due to the difference in the crystal structures (monoclinic *vs.* triclinic) as the phase transformation between brannerite and NiV_2O_6-type structure occurs when $x \geq 0.9$ in $Zn_{1-x}Co_xV_2O_6$ (Fig. 5, XRD). The corresponding variations in the color L*a*b parameters of the compositions in the series $Zn_{1-x}Co_xV_2O_6$ are listed in Table 6.

Further, MnV_2O_6 is known to exhibit a reversible phase transformation from brannerite to pseudo-brannerite at 540 °C [10]. To observe the influence of the structural changes on the optical properties, MnV_2O_6 was also prepared by air quenching from 700 °C. The powder XRD pattern of this sample (Fig. 11) is similar to the sample obtained by furnace cooling as the variation is expected only in the coordination geometry from VO_6 to VO_5. The DRUV-Vis reflectance spectra of these two samples are compared in Fig. 12 and it can be seen that the % reflectance is much lower for the air quenched sample when compared to that of MnV_2O_6 obtained by furnace cooling. The absorption edge showed a red shift in the case of air quenched sample and the estimated direct band gap values are 1.44 and 1.40 eV for samples obtained by furnace cooling and air quenching, respectively. The changes in the coordination geometry around V^{5+} ions influence the optical properties. Thus, our study reveals the possibility of tuning the colors of

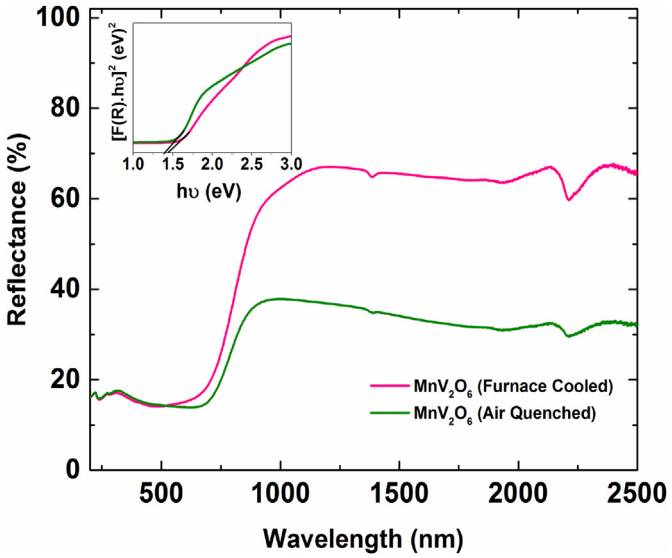

Fig. 12. DRUV-Vis reflectance spectra of MnV_2O_6 samples obtained by furnace cooling and air quenching. The inset shows the Tauc plot used for the estimation of direct band gap of these samples.

brannerite-type vanadium oxides through solid solutions to alter the local coordination environment of V^{5+} and phase transformation that results in a complex combination of change in the band gap, c. t. transitions, and introduction of d-d transitions. Further solid solutions in the brannerite oxides with other transition metal ions and their combinations will result in more color hues.

4. Conclusions

The optical properties of brannerite-type vanadium oxides MV_2O_6 (M = Ca, Mg, Mn, Co, Ni, Cu, or Zn) with marginal variations in the crystal structures have been studied. The optical band gap and O^{2-}-V^{5+} charge transfer (LMCT) transitions are responsible for the observed variations in the colors of samples containing metal ions with no d electrons (CaV_2O_6 and MgV_2O_6) and with d^{10} electrons (ZnV_2O_6). The introduction of transition metal ions with partially filled 3d orbitals alters the colors due to the presence of d-d transitions as observed in the case of $Ca_{0.99}M_{0.01}V_2O_6$ and $Zn_{0.99}M_{0.01}V_2O_6$ (M = Mn, Co, Ni, and Cu). The decreasing optical band gap, presence of d-d transitions of Mn^{2+}, MMCT transitions, and change in the coordination polyhedral (VO_5/VO_6) groups due to the phase transformation resulted in the change in the colors of samples in the solid solution series $Ca_{1-x}Mn_xV_2O_6$ (x = 0 - 1). Similarly, the presence of prominent d-d transition of Co^{2+}, band gap narrowing, and the structural changes resulted in the observed variation in the colors in $Zn_{1-x}Co_xV_2O_6$ (x = 0 - 1). Thus, the complex combination of changes in the band gap, LMCT and MMCT, and d-d transitions are responsible for tuning the colors of the brannertie-type vanadium oxides.

CRediT authorship contribution statement

N. Lakshminarasimhan: Conceptualization, Methodology, Supervision, Writing – original draft, Writing – review & editing. **Jun Li:** Writing – review & editing. **M.A. Subramanian:** Conceptualization, Methodology, Supervision, Writing – review & editing.

Declaration of competing interest

The authors declare that they have no known competing financial interests or personal relationships that could have appeared to influence the work reported in this paper.

Acknowledgements

The author NL acknowledges the United States-India Educational Foundation (USIEF) for the Fulbright-Nehru Academic and Professional Excellence Fellowship (2020–2021). The work done at Oregon State University is supported by US National Science Foundation Grant No. DMR-2025615.

References

[1] A.E. Smith, H. Mizoguchi, K. Delaney, N.A. Spaldin, A.W. Sleight, M.A. Subramanian, Mn^{3+} in trigonal bipyramidal coordination: a new blue chromophore, J. Am. Chem. Soc. 131 (2009) 17084–17086, https://doi.org/10.1021/ja9080666.

[2] J. Li, M.A. Subramanian, Inorganic pigments with transition metal chromophores at trigonal bipyramidal coordination: $Y(In,Mn)O_3$ blues and beyond, J. Solid State Chem. 272 (2019) 9–20, https://doi.org/10.1016/j.jssc.2019.01.019.

[3] H. Mizoguchi, A.W. Sleight, M.A. Subramanian, New oxides showing an intense blue color based on Mn^{3+} in trigonal-bipyramidal coordination, Inorg. Chem. 50 (2011) 10–12, https://doi.org/10.1021/ic102133z.

[4] R. Grajczyk, M.A. Subramanian, Structure-property relationships of $YbFe_2O_4$- and $Yb_2Fe_3O_7$-type layered oxides: a bird's eye view, Prog. Solid State Chem. 43 (2015) 37–46, https://doi.org/10.1016/j.progsolidstchem.2014.09.001.

[5] J. Li, S. Lorger, J.K. Stalick, A.W. Sleight, M.A. Subramanian, From serendipity to rational design: tuning the blue trigonal bipyramidal Mn^{3+} chromophore to violet and purple through application of chemical pressure, Inorg. Chem. 55 (2016) 9798–9804, https://doi.org/10.1021/acs.inorgchem.6b01639.

[6] D. Saraswathy, P.P. Rao, S. Sameera, V. James, A.K.V. Raj, Monoclinic $LaGa_xMn_xGe_2O_7$: a new blue chromophore based on Mn^{3+} in the trigonal bipyramidal coordination with longer apical bond lengths, RSC Adv. 5 (2015) 27278–27281, https://doi.org/10.1039/C5RA01714A.

[7] S. Tamilarasan, D. Sarma, M.L.P. Reddy, S. Natarajan, J. Gopalakrishnan, $YGa_{1-x}Mn_xO_3$: a novel purple inorganic pigment, RSC Adv. 3 (2013) 3199–3202, https://doi.org/10.1039/C2RA22400C.

[8] S. Tamilarasan, M.L.P. Reddy, S. Natarajan, J. Gopalakrishnan, Developing intense blue and magenta colors in α-$LiZnBO_3$: the role of 3d-metal substitution and coordination, Chem. Asian J. 11 (2016) 3234–3240, https://doi.org/10.1002/asia.201601124.

[9] S. Tamilarasan, S. Laha, S. Natarajan, J. Gopalakrishnan, Exploring the colour of 3d transition-metal ions in trigonal bipyramidal coordination: identification of purple-blue (CoO_5) and beige-red (NiO_5) chromophores in $LiMgBO_3$ host, Eur. J. Inorg. Chem. 2 (2016) 288–293, https://doi.org/10.1002/ejic.201501064.

[10] K. Mocała, J. Ziółkowski, Polymorphism of the bivalent metal vanadates MeV_2O_6 (Me = Mg, Ca, Mn, Co, Ni, Cu, Zn, Cd), J. Solid State Chem. 69 (1987) 299–311, https://doi.org/10.1016/0022-4596(87)90087-9.

[11] H.M. Buschbaum, M. Kobel, Zur kristallchemie von Oxovanadaten: γ-CoV_2O_6 and MnV_2O_6, J. Alloys Compd. 176 (1991) 39–46, https://doi.org/10.1016/0925-8388(91)90008-J.

[12] J.C. Bouloux, G. Perez, J. Galy, Structure cristalline des metavanadates CaV_2O_6 et CdV_2O_6 α. La transformation polymorphique CdV_2O_6 α - CdV_2O_6 β, Bull. Soc. Fr. Mineral. Cristallogr. 95 (1972) 130–133, https://doi.org/10.3406/bulmi.1972.6655.

[13] M. Watanabe, M. Muto, Y. Abe, T. Kaneko, A. Toda, K. Uematsu, T. Ishigaki, M. Sato, J. Koide, M. Toda, Y. Kudo, T. Masaki, D.-H. Yoon, S.-W. Kim, K. Toda, Synthesis of red-emissive CaV_2O_6 nanophosphor via a water assisted solid state reaction method, ECS J. Solid State Sci. Technol. 10 (2021) 106010, https://doi.org/10.1149/2162-8777/ac2e4c.

[14] B. Zoellner, E. Gordon, P.A. Maggard, A small band gap semiconductor, p-type MnV_2O_6, active for photocatalytic hydrogen and oxygen production, Dalton Trans. 46 (2017) 10657–10664, https://doi.org/10.1039/c7dt00780a.

[15] H.X. Dang, A.J.E. Rettie, C.B. Mullins, Visible-light-active NiV_2O_6 films for photoelectrochemical water oxidation, J. Phys. Chem. C 119 (2015) 14524–14531, https://doi.org/10.1021/jp508349g.

[16] W. Guo, W.D. Chemelewski, O. Mabayoje, P. Xiao, Y. Zhang, C.B. Mullins, Synthesis and characterization of CuV_2O_6 and $Cu_2V_2O_7$: two photoanode candidates for photoelectrochemical water oxidation, J. Phys. Chem. C 119 (2015) 27220–27227, https://doi.org/10.1021/acs.jpcc.5b07219.

[17] S.A.J. Kimber, J.P. Attfiled, Disrupted antiferromagnetism in the brannerite MnV_2O_6, Phys. Rev. B 75 (2007), 064406, https://doi.org/10.1103/PhysRevB.75.064406.

[18] A.N. Vasil'ev, L.A. Ponomarenko, A.I. Smirnov, E.V. Antipov, Y.A. Velikodny, M. Isobe, Y. Ueda, Short-range and long-range magnetic ordering in α−CuV_2O_6, Phys. Rev. B 60 (1999) 3021, https://doi.org/10.1103/PhysRevB.60.3021.

[19] Z. He, J.-I. Yamaura, Y. Ueda, W. Cheng, CoV_2O_6 single crystals grown in a closed crucible: unusual magnetic behaviors with large anisotropy and 1/3 magnetization plateau, J. Am. Chem. Soc. 131 (2009) 7554–7555, https://doi.org/10.1021/ja902623b.

[20] K. Momma, F. Izumi, Vesta 3 for three-dimensional visualization of crystal, volumetric and morphology data, J. Appl. Crystallogr. 44 (2011) 1272–1276, https://doi.org/10.1107/S0021889811038970.

[21] A.C. Larson, R.B. Von Dreele, General Structure Analysis System (GSAS) Report LAUR 86-748, Los Alamos National Laboratory, Los Alamos, 2004.

[22] B.H. Toby, EXPGUI, A graphical user interface for GSAS, J. Appl. Crystallogr. 34 (2001) 210–213.
[23] C. Calvo, D. Manolescu, Refinement of the structure of CuV_2O_6, Acta Crystallogr. B29 (1973) 1743–1745, https://doi.org/10.1107/S0567740873005455.
[24] S. Hansen, J. Nilsson, Coordination of vanadium(5+) in solid soutions MgV_2O_6-CaV_2O_6 and ZnV_2O_6-CaV_2O_6, Acta Chem. Scand. 50 (1996) 512–515, https://doi.org/10.3891/acta.chem.scand.50-0512.
[25] T.I. Krasnenko, O.A. Zabara, L.L. Surat, S.V. Strepetov, Investigation of the $Ca_{1-x}Mn_x(VO_3)_2$ solid solution, Inorg. Mater. 23 (1987) 1252–1254.
[26] R.D. Shannon, Revised effective ionic radii and systematic studies of interatomie distances in halides and chaleogenides, Acta Crystallogr. A32 (1976) 751–767, https://doi.org/10.1107/S0567739476001551.
[27] G.D. Andreetti, G. Calestani, A. Montenero, M. Bettinelli, Refinement of the crystal structure of ZnV_2O_6, Z. Kristallogr. 168 (1984) 53–58, https://doi.org/10.1524/zkri.1984.168.14.53.
[28] D. von Dreifus, R. Pereira, A.D. Rodrigues, E.C. Pereira, A.J.A. de Oliveira, Sol gel synthesis of triclinic CoV_2O_6 polycrystals, Ceram. Intl. 44 (2018) 19397–19401, https://doi.org/10.1016/j.ceramint.2018.07.171.
[29] P. Atkins, T. Overton, J. Rourke, M. Weller, F. Armstrong, M. Hagerman, Inorganic Chemistry, fifth ed., Oxford University Press, 2010, p. 642.
[30] P.A. Cox, The Electronic Structure and Chemistry of Solids, Oxford University Press, Oxford, 1987.
[31] M. Lasserus, D. Knez, F. Lackner, M. Schnedlitz, R. Messner, D. Schennach, G. Kothleitner, F. Hofer, A.W. Hauser, W.E. Ernst, Synthesis of nanosized vanadium(V) oxide clusters below 10 nm, Phys. Chem. Chem. Phys. 21 (2019) 21104–21108, https://doi.org/10.1039/C9CP04357H.
[32] K. Schneider, Optical properties and electronic structure of V_2O_5, V_2O_3 and VO_2, J. Mater. Sci. Mater. Electron. 31 (2020) 10478–10488, https://doi.org/10.1007/s10854-020-03596-0.
[33] G.R. Rossman, R.D. Shannon, R.K. Waring, Origin of the yellow color of complex nickel oxides, J. Solid State Chem. 39 (1981) 277–287, https://doi.org/10.1016/0022-4596(81)90261-9.
[34] L.G.J. De Haart, G. Blasse, The application of nickel molybdate and nickel vanadates as photoanodes in a photoelectrochemical cell, Mater. Chem. Phys. 12 (1985) 545–550, https://doi.org/10.1016/0254-0584(85)90040-9.
[35] Md S. Islam, H. Kabir, Y. Inagaki, A.R. Sarker, Comparative study of the conductivity of synthesized bivalent vanadates CaV_2O_6 and MnV_2O_6, J. Alloys Compd. 829 (2020) 1–5, https://doi.org/10.1016/j.jallcom.2020.154499, 154499.
[36] S. Dey, R.A. Ricciardo, H.L. Cuthbert, P.M. Woodward, Metal-to-metal charge transfer in AWO_4 (A = Mg, Mn, Co, Ni, Cu, or Zn), Inorg. Chem. 53 (2014) 4394–4399, https://doi.org/10.1021/ic4031798.
[37] B. Serment, L. Corucho, A. Demourgues, G. Hadziioannou, C. Brochon, E. Cloutet, M. Gaudon, Tailoring the chemical composition of $LiMPO_4$ (M = Mg, Co, Ni) orthophosphates to design new inorganic pigments from magenta to yellow hue, Inorg. Chem. 58 (2019) 7499–7510, https://doi.org/10.1021/acs.inorgchem.9b00715.
[38] B.A. Duell, J. Li, M.A. Subramanian, Hibonite blue: a new class of intense inorganic blue colorants, ACS Omega 4 (2019) 22114–22118, https://doi.org/10.1021/acsomega.9b03255.